Processing and Application of Ceramics 17 [4] (2023) 428–435
https://doi.org/10.2298/PAC2304428K

# Double perovskite $Nd_2FeTiO_6$ ceramics: Structural and electrical properties

Mrityunjay Kumar[1,2], Sumit K. Roy[3], Rahul K. Singh[2], Kamal Prasad[4,*]

[1] *Department of Physics, Govt. Naveen College, Tokapal, Bastar 494442, India*
[2] *University Department of Physics, Ranchi University, Ranchi 834009, India*
[3] *Department of Physics, St. Xavier's College, Ranchi 834001, India*
[4] *University Department of Physics, T.M. Bhagalpur University, Bhagalpur, 812007, India*

Received 27 March 2023; Received in revised form 27 August 2023; Received in revised form 30 November 2023; Accepted 11 December 2023

## Abstract

*Because of their high stability, innocuous behaviour, outstanding electric properties and multi-functionality, lead-free double perovskites have emerged as a promising alternative to lead-based perovskites. We present here the structural, microstructural, dielectric and electrical properties of a newly synthesized double perovskite $Nd_2FeTiO_6$ (NFTO). The Rietveld refinement of its X-ray diffraction pattern revealed a monoclinic structure with space group $P12_1/c1$. The oxide exhibits a temperature-independent dielectric constant and dielectric loss at low temperatures (below 200 °C) making the compound a suitable candidate for fabricating thermally stable capacitors. The AC conductivity was investigated using the Jonscher's universal power law, and it was inferred that the conduction process is caused by the Correlated Barrier Hopping (CBH) mechanism. Furthermore, frequency dependent AC conductivity also revealed the NTCR nature of the NFTO compound.*

***Keywords:*** *perovskites, lead-free ceramic, microstructure, dielectric constant, impedance*

## I. Introduction

Researchers' attention has recently been drawn to lead-free double perovskite materials with the general formula $A_2BB'O_6$ (A denotes alkaline or rare earth metals and B and B′ sites are occupied by transition metals), due to their sublime and intriguing properties and technological applications in a variety of electronic devices, including photovoltaics, sensors, magnetic memory, energy storage devices, spintronics etc. The double perovskite materials, with a general chemical formula $AA'BB'O_6$, are the combination of two single perovskites $ABO_3$ and $A'B'O_3$ where A and A′ correspond to alkaline or rare earth cations. However, if A-sites are occupied by the same cation, then the compound has the formula $A_2BB'O_6$. The structure of double perovskite ($A_2BB'O_6$) consists of two octahedrons ($BO_6$ and $B'O_6$) which multiply in all three directions such that each $B'O_6$ octahedron is connected only to $BO_6$ octahedra and vice versa. It is seen that double perovskite with two rare earth metals at A-sites and two different transition metals at B-sites provide better flexibility and catalytic properties compared to single perovskites. Besides, the presence of transition metal cations at B- and B′-sites with $3d/4d$ valence electrons delivers superior magnetic properties.

Many double perovskites have been prepared and studied so far such as $La_2CoMnO_6$, $Sr_2CrWO_6$, $Y_2CoMnO_6$, etc. Due to their improved magnetic properties, lately research has been concentrated on a particular kind of double perovskite with the B- and B′-sites containing Fe, Mn, Ti, Ni, etc. Further, Nd-based perovskite compounds have drawn a lot of interest due to their promising features, such as multiferroic and other $NdFeO_3$ properties that are widely reported in the literature [1–5]. Kumar *et al.* [6] reported the formation of a single phase orthorhombic $Ti^{4+}$-ion substituted $NdFeO_6$ that displayed the antiferromagnetic ordering. Ghrib *et al.* [7] studied the structural, dielectric, optical and magnetic properties of $A_2FeTiO_6$ (A = Mg, Cu, Zn). They observed that $Mg_2FeTiO_6$ exhibited a

---

[*] Corresponding author: tel: +91 641 2501699,
e-mail: *prasad_k@tmbuniv.ac.in; k.prasad65@gmail.com*

high dielectric constant and very low loss tangent that makes it suitable for radio frequency and microwave applications, whereas $Zn_2FeTiO_6$ with low loss tangent was reported to be suitable for high-frequency applications. Other studies carried out by Boudad *et al.* showed that $RBaFeTiO_6$ (R = La, Eu) [8] and $RBaFeTiO_6$ (R = Pr, Nd) [9] have a cubic ($Pm\bar{3}m$) structure with low value of loss tangent in the high-frequency range that shows their potential for using them in different electrical and/or electronic industries. In another study, Iben Nassar *et al.* [10] reported that $LaPbFeTiO_6$ crystallizes in a rhombohedral structure ($R\bar{3}C$) having a high value of dielectric permittivity and potential to be used in capacitor applications. The structural and morphological studies of $SrNdFeTiO_6$ were carried out by Sanghi *et al.* [11], whereas Abhirami *et al.* [12] explored the magnetic behaviour of $La^{3+}$-ion substituted $Nd_2FeMnO_6$ and confirmed its super-paramagnetic behaviour. The polycrystalline compound $La_{0.5}Nd_{0.15}Ca_{0.35}MnO_3$ was prepared by Rajan *et al.* [13] by conventional solid-state reaction method. The compound revealed the formation of orthorhombic perovskite sample with *Pbnm* space group symmetry and possessed high magnetoresistance. Lyu *et al.* [14] synthesized the lead-free double perovskite $Cs_2AgBiBr_6$ films by tuning rare earth $Nd^{3+}$-content and investigated the resistive memory properties. They observed that the compound exhibited a typical write-once-read-many-times (WORM) behaviour with low on-set voltage and long retention time. In a recent study, Irfan *et al.* [15] investigated the structural, electronic and magnetic properties of the double perovskites $RE_2NiCrO_6$ (RE = Ce, Pr and Nd) using the experimental route and density functional theory approach.

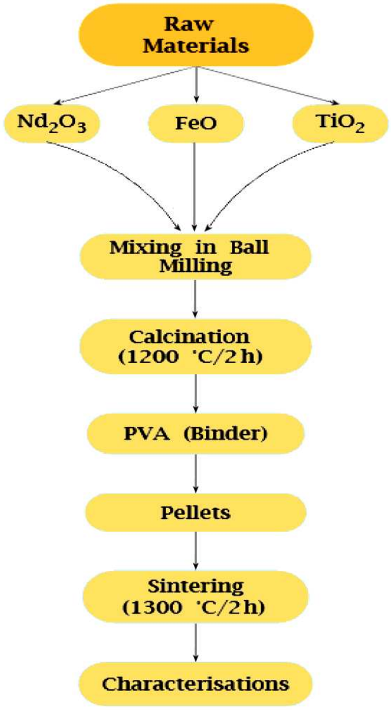

**Figure 1. Synthesis scheme of double perovskite oxide $Nd_2FeTiO_6$**

A thorough review of the literature revealed that, to the best of our knowledge, no work has been done on a solid-state reaction method synthesis of the double perovskite oxide $Nd_2FeTiO_6$ (abbreviated as NFTO). Accordingly, structure (X-ray diffraction), microstructure (FE-SEM), dielectric and impedance studies have thus been addressed in this work.

## II. Experimental

Polycrystalline $Nd_2FeTiO_6$ samples were synthesized by a solid-state reaction process (Fig. 1). Stoichiometric amounts of AR grade $Nd_2O_3$ (Merck), FeO (Sigma Aldrich) and $TiO_2$ (Alfa Aesar) were taken and mixed in an agate-mortar and pestle. To enhance the uniformity, reactants were further mixed in a ball mill for 20 min at 200 rpm keeping powder to ball ratio at 1:15. Thereafter, the mixture was calcined at 1200 °C for 3 h. The X-ray diffraction technique (XRD) was used to verify that the reaction had been finished and the desired compound had formed. The as-calcined powder with PVA as the binder was used to create pellets with dimensions of 10 mm in diameter and 0.96 mm in thickness which were then sintered at 1300 °C for 2 h.

X-ray diffractometer (Rigaku Miniflex 600) used $CuK_\alpha$ radiation ($\lambda$ = 1.5405 Å) and a wide range of Bragg angles ($20° \le 2\theta \le 80°$) to record the XRD data of the sintered pellet. The micrographs (fractured surface) of the NFTO double perovskite were acquired using a field emission scanning electron microscope (SEM JEOL-JSM840A, Japan). The Ag conductive paste was coated on each side of the polished sintered pellet for electrical measurements. A computer-controlled LCR Hi-Tester (HIOKI 3532-50, Japan) was used for this purpose and the data were acquired as a function of frequency (100 Hz–1 MHz) at various temperatures (35–500 °C). This device was interfaced with a microprocessor-controlled temperature controller (DPI-1100, Sartech Intl, India).

## III. Results and discussion

Good predictive tool for the determination of the structure of the family of double perovskites is the tolerance factor given by the following equation:

$$t = \frac{r_A + r_O}{\sqrt{2}\left(\frac{r_B + r_{B'}}{2} + r_O\right)} \tag{1}$$

where, $r_A$, $r_B$ and $r_{B'}$ are the ionic radii of the cations at A-, B- and B′-sites of the double perovskite and $r_O$ is the radius of the oxygen ion [16,17]. According to this, the tolerance factor is 1 for an ideal cubic structure. For other crystal structures, literature provides a generalization regarding the tolerance factor of the double perovskite family members and if t lies in range: i) $1.05 > t > 1.00$ the structure should be cubic; ii) $1.00 >$

$t > 0.97$ compounds have tetragonal structure and iii) $t < 0.97$ the compound will have either monoclinic or orthorhombic structure [16–19]. The value of $t$ for NFTO was calculated to be 0.902 and thus the structure is expected to be either monoclinic or orthorhombic. To confirm the crystal structure, XRD data of the NFTO was analysed and the peaks can be indexed as monoclinic as well as orthorhombic. Rietveld refinement was performed with respect to both crystal structures. NFTO indexed to monoclinic crystal structure exhibited better fit. Based on $\chi^2$, $R_f$ and $R_b$, the Rietveld refinement quality was assessed. It can be seen in Fig. 2 that there is a fair correlation between the calculated and observed XRD profiles, which points to the formation of the compound with a monoclinic structure and the space group $P12_1/c1$. Peaks detected at Bragg angles 21.5°, 28.5°, and 30.5° in the XRD pattern do not correspond to any Bragg positions, suggesting the presence small amount of a secondary phase or structural disorder. Table 1 displays the obtained lattice parameters, atom positions and reliability factors. Using the cell parameters presented in Table 1 we have modelled a single-ordered NFTO unit cell using VESTA software (Fig. 3). The unit cell of NFTO consists of two Fe and two Ti atoms within the octahedron cage of O atoms. Also, the Nd atom accommodates itself in the gap of $FeO_6$ and $TiO_6$ octahedron. The XRD data was also used to determine the crystallite size using the Debye Scherrer formula, which comes out to be about 54 nm.

Figure 4 shows the FESEM micrographs of fractured surface of the sintered NFTO ceramics at two magnifications. The sample's homogeneous appearance and uniform distribution of grains of various sizes and shapes indicate that the double perovskite was synthesized in a polycrystalline state. Also, the sample contains pores apart from some localized agglomerations of grains which indicates its formation fairly dense structure.

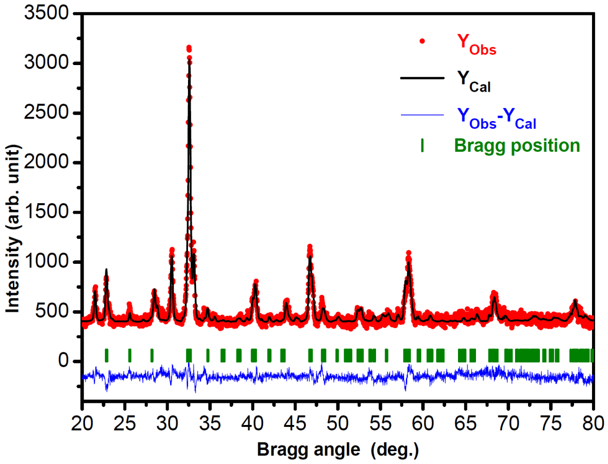

**Figure 2. Rietveld refined XRD pattern of $Nd_2FeTiO_6$ ceramics**

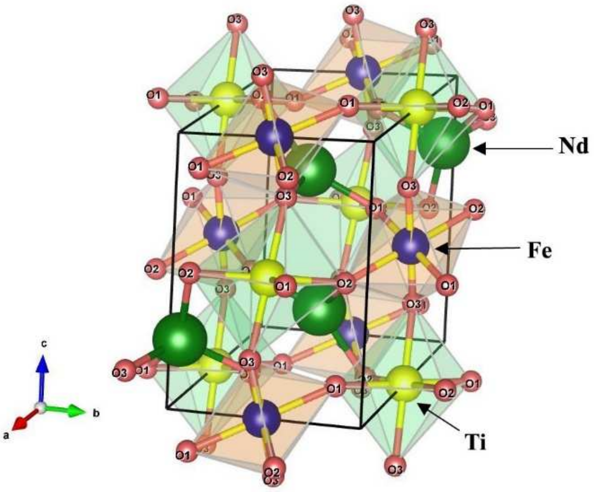

**Figure 3. Crystal structure of $Nd_2FeTiO_6$ ceramics**

**Table 1. Structure parameter of $Nd_2FeTiO_6$ ceramics**

| | | | |
|---|---|---|---|
| Space group | $P12_1/c1$ | $V$ [Å$^3$] | 233.7373 |
| $a$ [Å] | 5.5218(7) | $\alpha$ | 90° |
| $b$ [Å] | 5.4658(7) | $\beta$ | 125.37(1)° |
| $c$ [Å] | 9.498(2) | $\gamma$ | 90° |
| *GOF* | 1.08297 | *R* (Weighted profile) [%] | 7.48111 |
| *R* (profile) [%] | 5.98935 | *R* (Bragg) [%] | 4.00179 |
| $Fe–O_3$ [Å] | 1.67 | $O_3–Fe–O_1$ | 99.4° |
| $Fe–O_2$ [Å] | 2.13 | $O_2–Fe–O_3$ | 103.8° |
| $Fe–O_1$ [Å] | 2.10 | $O_1–Fe–O_2$ | 81.2° |
| $Ti–O_3$ [Å] | 2.19 | $O_3–Ti–O_1$ | 101.7° |
| $Ti–O_2$ [Å] | 2.04 | $O_2–Ti–O_3$ | 99.7° |
| $Ti–O_1$ [Å] | 2.00 | $O_1–Ti–O_2$ | 84.9° |
| $Nd–O_3$ [Å] | 2.25 | $O_3–Nd–O_1$ | 100.4° |
| $Nd–O_2$ [Å] | 2.41 | $O_2–Nd–O_3$ | 80.3° |
| $Nd–O_1$ [Å] | 2.11 | $O_1–Nd–O_2$ | 151.8° |

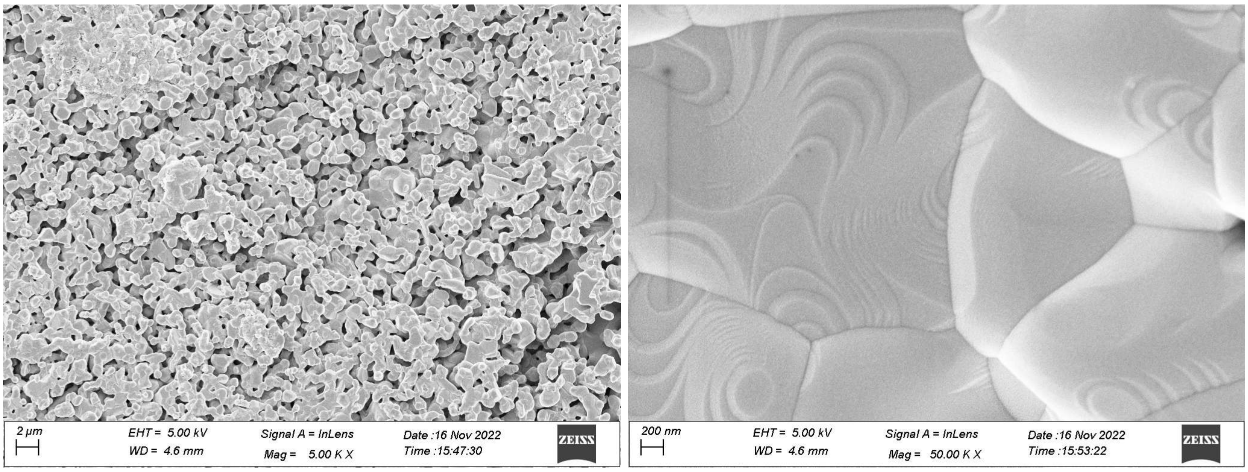

**Figure 4. Field emission scanning electron micrograph of $Nd_2FeTiO_6$ double perovskite**

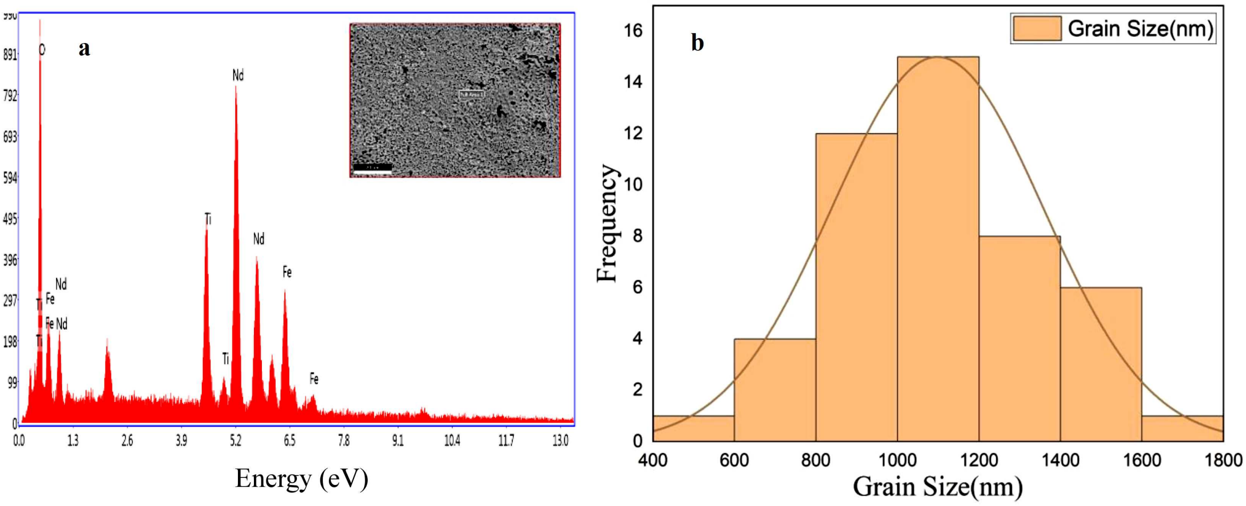

**Figure 5. (a) EDS pattern of NFTO double perovskite and (b) Distribution of grain size**

Figure 5a shows the EDS spectrum of the prepared double perovskite. All of the patterns' peaks have been precisely identified and belong to the components of present double perovskite, demonstrating its purity during formation. The Gaussian distribution (Fig. 5b) over grain size suggests the most probable grain size to be 1.07 µm.

Figures 6a and 6b display the dependence of the real part of the dielectric constant ($\varepsilon'$) with temperature for lower (1, 5, 10 and 50 kHz) and for higher frequencies (0.1, 0.5 and 1 MHz), respectively. It is seen that for all frequencies, values of $\varepsilon'$ remain almost constant in the low-temperature region and start increasing as temperature increases. The value of $\varepsilon'$ is nearly constant ($\approx$30) up to ~180 °C for all frequencies. The characteristic peak corresponding to the ferro-paraelectric phase transition is observed at 370 °C for all frequencies. The value of $\varepsilon'$ is observed to be higher at lower frequencies; this is due to the accretion of charges at grain boundaries [20,21]. The increasing trend of dielectric constant at higher temperatures can be attributed to space charges and the sample's conductivity. As temperature rises, charge carriers become more mobile, which increases the samples' conductivity and polarisation and raises the dielectric constant [22].

The variation of dielectric loss ($\tan\delta$) as a function of temperature at lower and higher frequencies is shown in Figs. 6c and 6d, respectively. The nature of the $\tan\delta$ curve is similar to that of $\varepsilon'$ and it is almost constant (< 1) again up to temperature 180 °C and then starts increasing with temperature. It attains a maximum at 365 °C for all frequencies which corresponds to the phase transition temperature ($T_c$). The increasing trend of dielectric loss after transition temperature can be attributed to space charge polarisation [20,22]. The frequency and temperature independent $\varepsilon'$ and $\tan\delta$ (below 180 °C), over a wide frequency range (500 Hz–1 MHz), make the material suitable for thermally stable capacitors [23]. The room temperature value of $\varepsilon'$ and $\tan\delta$ is recorded to be 32 and 0.0805, respectively, at 1 kHz which suggests that the material may be useful for capacitor applications. The temperature dependence of the dielectric constant and loss tangent of the double perovskite NFTO is in line with other double perovskites reported in the literature [24–26], with a contrast that the room temperature dielectric constant of the NFTO

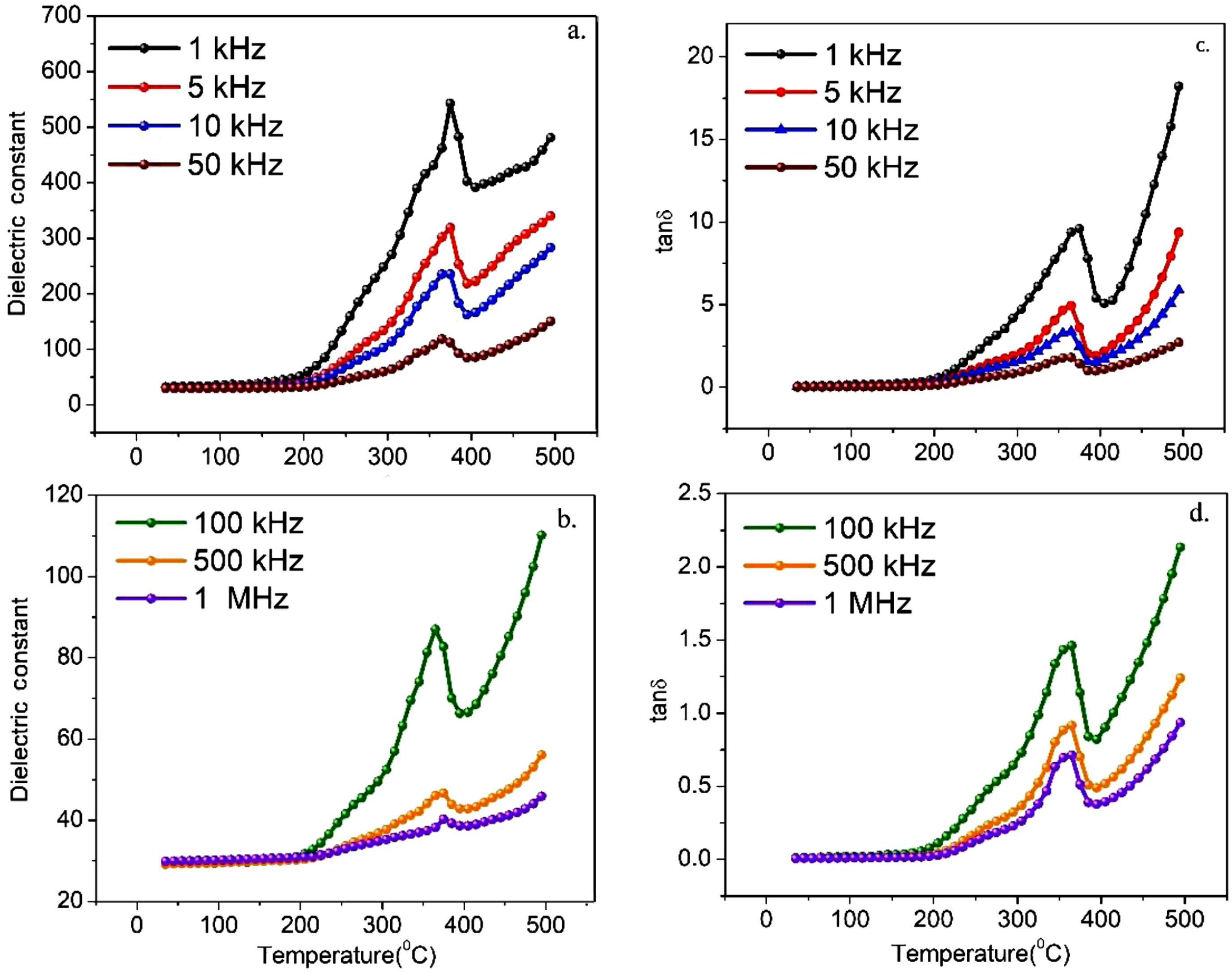

**Figure 6. Temperature dependence of dielectric constant (a and b) and loss tangent (c and d) of $Nd_2FeTiO_6$ ceramics at different frequencies**

is low compared to other reported double perovskites. The low value of the effective dielectric constant can be attributed to the distortion of the electric field lines close to the voids and/or pore surfaces, which lowers the polarization and, consequently, the dielectric constant.

The change of $\varepsilon'$ and $\tan\delta$ with frequencies at different temperatures is presented in Fig. 7. It is evident from the plot that $\varepsilon'$ as well as $\tan\delta$ have higher values in the low-frequency range and that their values steadily decrease as frequency increases, which may be related to a decrease in the space charge polarization. Aggregation of charges close to grain boundaries with high resistance will result in space charge polarisation. A potential barrier is produced by space charge polarisation close to grain boundaries. Thus, the gathering of charges at grain boundaries consequently exhibits high values of $\varepsilon'$ in the lower frequency regime [16,21]. The dielectric constant decreases as frequency rises because the dipoles are unable to arrange themselves in the direction of the rapidly changing electric field. At higher frequencies, neither of the parameters ($\varepsilon_r$ and $\tan\delta$) changes, possibly because charge carriers are unable to accumulate at the interface within a very short period of time.

The real ($M'$) and imaginary ($M''$) parts of electric modulus were obtained from the dielectric data, utilizing the relation:

$$M^*(\omega) = M'(\omega) + iM''(\omega) = \frac{\varepsilon'(\omega)}{|\varepsilon(\omega)|^2} + \frac{i\varepsilon''(\omega)}{|\varepsilon(\omega)|^2} \quad (2)$$

Figure 8 shows how $M'$ and $M''$ depend on frequency at various temperatures. At high temperatures and low frequencies, the value of $M'$ nearly equals zero, indicating the absence of electrode polarisation [27,28]. At higher frequencies, $M'$ starts to show saturation nature which can be associated with the conduction process because of the movement of charge carriers (ions) over a small distance (short-range conduction due to ions) [28,29]. The values of $M'$ decrease with the rise in temperature indicating an improvement in the conductivity of the sample [29]. From the graph of $M''$ vs. frequency, it can be noted that it starts increasing with frequency and attains their respective relaxation peaks. At temperatures between 300 and 500 °C, very distinct relaxation peaks are visible in the $M''$ spectra, along with a stepwise shift from low to high values in $M'$. Charge carriers are mobile over long distances prior to the peak maximum of $M''$ *vs.* frequency variation and over short distances

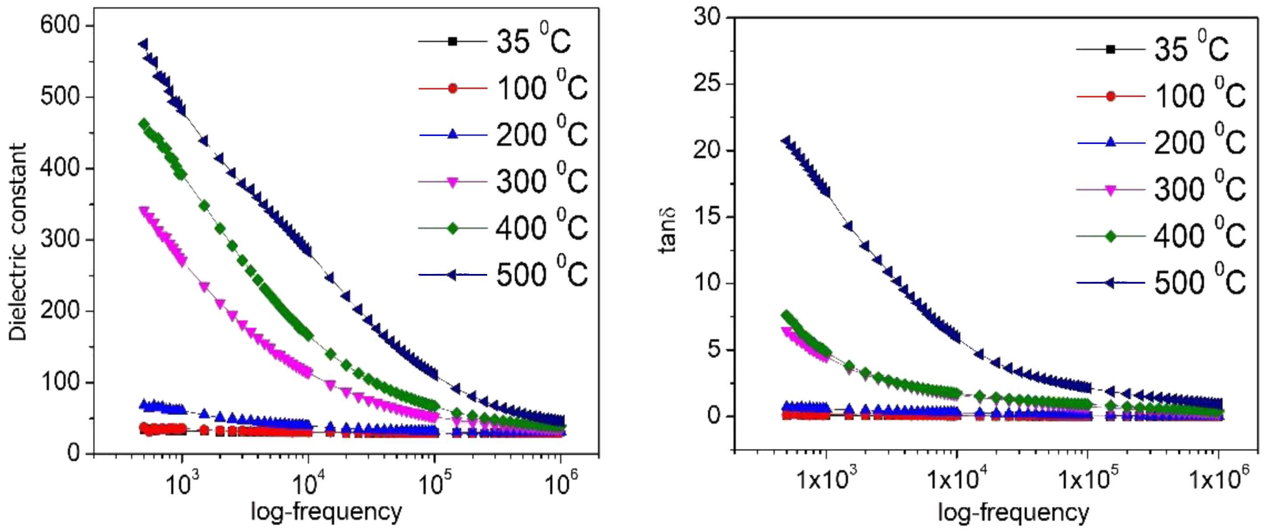

**Figure 7. Frequency dependence of dielectric constant and loss tangent of $Nd_2FeTiO_6$ double perovskite oxide at different temperatures**

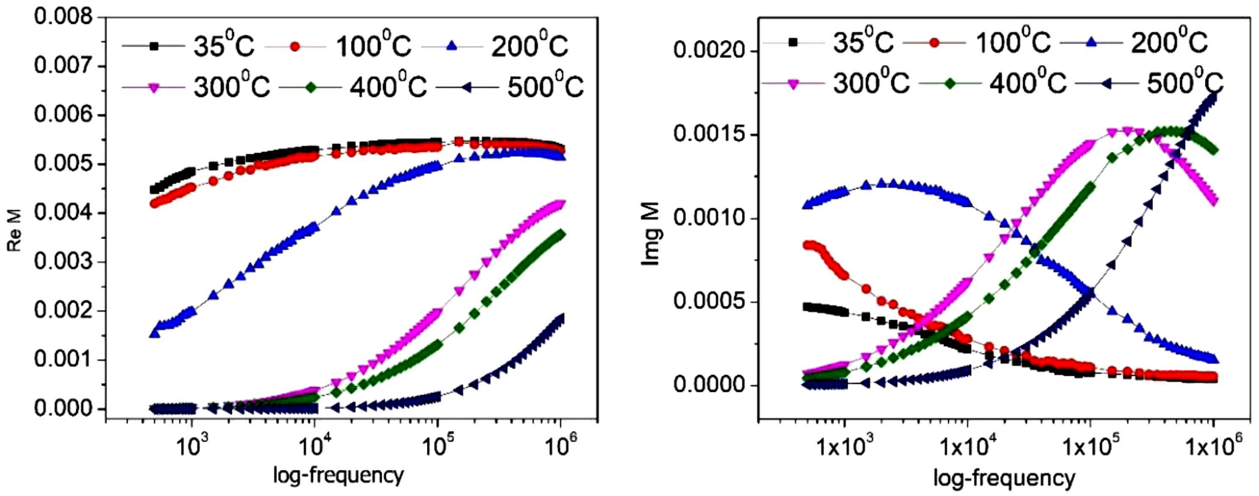

**Figure 8. Variation of real and imaginary parts of electric modulus of $Nd_2FeTiO_6$ double perovskite oxide with frequency at different temperatures**

following the peak maximum of ″M *vs*. frequency [30]. There is a shift of the peaks towards higher frequency as the temperature increases which can be associated with the dielectric relaxation process [31]. The material's non-Debye relaxation is supported by the asymmetry in peak broadening, which reflects the dispersion of relaxation times with various time constants [31].

To comprehend the frequency dependency of the material's electrical characteristics as well as to understand the nature of the charge carriers, AC conductivity ($\sigma_{AC}$) studies were undertaken. The values of AC conductivity were calculated from the formula $\sigma_{AC} = \varepsilon' \cdot \varepsilon_0 \cdot \cdot \omega \cdot \tan\delta$, where $\varepsilon_0$ and $\omega$ are the permittivity of free space and angular frequency, respectively. Figure 9 depicts the investigation into the frequency dependence of AC conductivity. It can be seen that conductivity is almost frequency-independent (plateau region) in the low-frequency region at lower temperatures and dispersive in nature at higher temperatures. However,

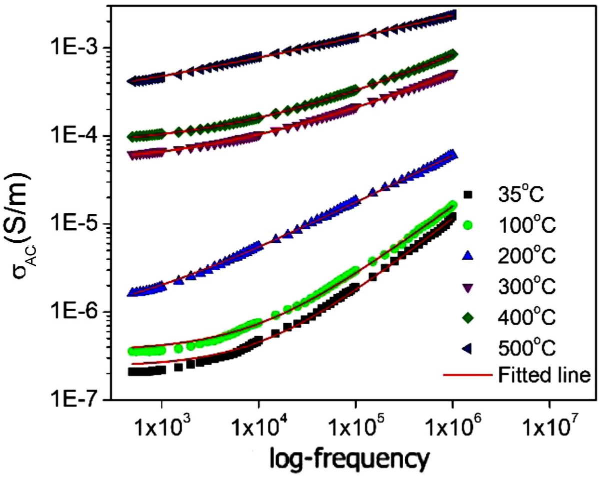

**Figure 9. Frequency dependence of AC conductivity of $Nd_2FeTiO_6$ double perovskite at selected temperatures**

**Table 2. Temperature dependence of frequency coefficient and frequency exponent in the Jonscher's power law for $Nd_2FeTiO_6$ double perovskite**

| Temperature [ °C] | $A$ | $n$ |
|---|---|---|
| 35 | $1.59 \times 10^{-11}$ | 0.86116 |
| 100 | $4.93 \times 10^{-11}$ | 0.80908 |
| 200 | $1.16 \times 10^{-8}$ | 0.54595 |
| 300 | $3.40 \times 10^{-7}$ | 0.46154 |
| 400 | $4.42 \times 10^{-7}$ | 0.47585 |
| 500 | $3.28 \times 10^{-5}$ | 0.26925 |

for higher temperature regions it becomes invariant of frequency. Explanation of the frequency dependence of conductivity can be given by the universal power law developed by the Jonscher:

$$\sigma_{AC} = \sigma_{DC} + A \cdot \omega^n \tag{3}$$

where $n$ is the exponent factor and $A$ is the extent of polarizability. The values of both $A$ and $n$ are estimated from a linear least-squares fitting approach which are presented in Table 2.

For a Debye type model value of $n = 1$ while for non-Debye type model value of $n$ may be less than or greater than 1. The obtained values of $n$ ($< 1$) suggest a non-Debye type conduction process [28]. Different models have been proposed, such as: i) the correlated barrier-hopping (CBH) model (which predicts that conductivity will decrease with rising temperature), ii) the quantum mechanical tunnelling model (which predicts that conductivity will remain constant with rising temperature), iii) the non-overlapping small polaron tunnelling (NSPT) model (which predicts that conductivity will increase with rising temperature) and iv) the overlapping large polaron tunnelling (OLPT) model (which predicts that conductivity will initially decrease with temperature, reach a minimum, and then increase). It can be noticed that the exponent factor $n$ shows a declining trend with temperature (Table 2) which indicates that the CBH model best explains the conduction mechanism of the NFTO ceramics [28,32]. The rise in the value of $\sigma_{AC}$ as the temperature increases demonstrates the sample's NTCR (negative temperature coefficient of resistance) property.

## IV. Conclusions

The polycrystalline NFTO ceramics was prepared using a high-temperature solid-state reaction process. X-ray diffraction analysis revealed that the compound has a monoclinic structure with the space group $P12_1/c1$. The crystallite size calculated using the Scherrer's formula is found to be 54 nm. The microstructural (FE-SEM) analysis revealed uniform distribution of grains of different shapes and sizes with small voids present at the surface. All required elements were present in the sample confirmed by the EDAX spectrum. From room temperature to 180 °C both dielectric constant and dielectric loss of the sample were found to be constant for the broad frequency range (500 Hz–1 MHz) which makes the compound very much suitable for thermally stable capacitors. The room temperature value of the dielectric constant and loss tangent at 1 kHz are 32 and 0.0805 respectively. The dependence of AC conductivity on frequency was investigated using the Jonscher's universal power law. The value of the exponent factor ($n$ of $\omega^n$) always remains less than 1, indicating the motion of charge carriers with sudden hopping. The plot of the exponent factor with temperature tells us that the conduction process follows the CBH model. The increasing value of AC conductivity with temperature demonstrated a negative temperature coefficient of resistance (NTCR) of the sample which further opens a new dimension to study its semiconducting behaviour.

## References

1. M. Khorasani-Motlagh, M. Noroozifar, M. Yousefi, S. Jahani, "Chemical synthesis and characterization of perovskite $NdFeO_3$ nanocrystals via a co-precipitation method", *Int. J. Nanosci. Nanotechnol.*, **9** (2013) 7–14.
2. J. Shanker, G.N. Rao, K. Venkataramana, D.S. Babu, "Investigation of structural and electrical properties of $NdFeO_3$ perovskite nanocrystalline", *Phys. Lett. A*, **382** (2018) 2974–2977.
3. Z. Anajafi, M. Naseri,, S. Marini C, Espro, D. Iannazzo, S.G. Leonardi, G. Neri, "$NdFeO_3$ as a new electrocatalytic material for the electrochemical monitoring of dopamine", *Analyt. Bioanalyt. Chem.*, **411** (2019) 7681.
4. N. Aparnadevi, K.S. Kumar, M. Manikandan, D.P. Joseph, C. Venkateswaran, "Room temperature dual ferroic behaviour of ball mill synthesized $NdFeO_3$ orthoferrite", *J. Appl. Phys.*, **120** (2016) 034101.
5. A.T. Nguyen, T.A. Nguyen, V.O. Mittova, H.D. Ngo, M.L.P. Le, D.Q. Nguyen, T.L. Nguyen, "Facile co-precipitated synthesis of $NdFeO_3$ perovskite nanoparticles for lithium-ion battery anodes", *J. Mater. Sci. Mater. Electron.*, **33** (2022) 19082–19091.
6. S. Kumar, S. Kaur, M. Arora, S. Sapna, S. Sharma, J. Pal, A. Singh, "Structural, microstructural and magnetic properties of B-site $Ti^{4+}$ substituted $NdFeO_3$ solid solutions", *AIP Conf. Proc.,* **2220** (2020) 030006.
7. T. Ghrib, F. Ercan, T.S. Kayed, T.H. Flemban, M. Yıldız, O. Kaygili, İ. Ercan, "Structural, optical, dielectric and magnetic properties of double perovskite oxides $A_2FeTiO_6$ (A = Zn, Mg, Cu) nanopowders", *Arab. J. Sci. Eng.*, **47** (2022) 7609–7620.
8. L. Boudad, M. Taibi, A. Belayachi, M. Abd-Lefdil, "Structural, morphological, dielectric and optical properties of double perovskites $RBaFeTiO_6$ (R = La, Eu)", *RSC Adv.*, **11** (2021) 40205–40215.
9. L. Boudad, M. Taibi, A. Belayachi, M. Abd-Lefdil, "Sol-gel synthesis and characterization of novel double perovskites $RBaFeTiO_6$ (R = Pr, Nd)", *Ceram. Int.*, **48** (2022) 6087–6096.
10. K. Iben Nassar, M. Slimi, N. Rammeh, S.S. Teixeira, M.P.F. Graça, "Structural and electrical properties of double perovskite oxide $LaPbFeTiO_6$ synthesized by a sol-gel process", *Appl. Phys. A*, **127** (2021) 940.
11. Vibha, S. Sanghi, A. Agarwal, M. Chauhan, E. Arya, A. Kumari, S. Kaushik, P. Sharma, "Crystal structure deter-

mination, XRD peak profile analysis and morphological study of double perovskite $SrNdFeTiO_6$", *Mater. Today Proc.*, **82** (2023) 79–84.

12. S. Abhirami, S.S. Basha, C. Vandalur, "Effect of trivalent lanthanide substitution on novel $Nd_2FeMnO_6$ double perovskite compounds", *Solid State Technol.*, **64** (2021) 4125–4141.
13. S. Rajan, A.K. Kumar, J. Isac, "Colossal magnetoresistance of Nd-doped $LaCaMnO_3$ polycrystalline ceramics", *Process. Appl. Ceram.*, **15** (2021) 95–99.
14. C. Lyu, C. Liu, H. Min, X. Shi, R. Jiang, Z. Ao, L. Wang, "Rare earth Nd-doping lead-free double perovskite $Cs_2AgBiBr_6$ films with improved resistive memory performance", *J. Alloys Compd.*, **913** (2022) 165300.
15. M. Irfan, G. Murtaza, N. Muhammad, S. Tahir, H.H. Raza, B. Sabir, M. Iftikhar, S. Sharif, "Experimental and theoretical studies of structural, electronic and magnetic properties of $RE_2NiCrO_6$ (RE = Ce, Pr and Nd) double perovskites", *Phys. E Low-dimens. Syst. Nanostruct.*, **148** (2023) 115635.
16. R. Das, R.N.P. Choudhary, "Studies of structural, dielectric relaxor and electrical characteristics of lead-free double perovskite: $Gd_2NiMnO_6$", *Solid State Sci.*, **87** (2019) 1–8.
17. M.T. Anderson, K.B. Greenwood, G.A. Taylor, K.R. Poeppelmeier, "B-cation arrangements in double perovskites", *Prog. Solid State Chem.*, **22** (1993) 197–233.
18. F. Gheorghiu, L. Curecheriu, I. Lisiecki, P. Beaunier, S. Feraru, M.N. Palamaru, L. Mitoseriu, "Functional properties of $Sm_2NiMnO_6$ multiferroic ceramics prepared by spark plasma sintering", *J. Alloys Compd.*, **649** (2015) 151–158.
19. M.D.I. Bhuyan, S. Das, M.A. Basith, "Sol-gel synthesized double perovskite $Gd_2FeCrO_6$ nanoparticles: Structural, magnetic and optical properties", *J. Alloys Compd.*, **878** (2021) 160389.
20. N. Panda, B.N. Parida, R. Padhee, R.N.P. Choudhary, "Dielectric and electrical properties of the double perovskite $PbBaBiNbO_6$", *J. Electron. Mater.*, **44** (2015) 4275–4282.
21. R. Das, R.N.P. Choudhary, "Synthesis and characterization of rare-earth ion-based double perovskite: $Gd_2CoMnO_6$", *J. Mater. Sci. Mater. Electron.*, **31** (2020) 12743–12755.
22. B.K. Barick, K.K. Mishra, A.K. Arora, R.N.P. Choudhary, D.K. Pradhan, "Impedance and Raman spectroscopic studies of $(Na_{0.5}Bi_{0.5})TiO_3$", *J. Phys. D Appl. Phys.*, **44** (2011) 355402.
23. R.A. Bucur, A.I. Bucur, S. Novaconi, I. Nicoara, "$BaSnO_3$ based thermally stable capacitors", *J. Alloys Compd.*, **542** (2012) 142–146.
24. J.W. Chen, K.R. Chiou, A.C. Hsueh, C.R. Chang, "Dielectric relaxation of the double perovskite oxide $Ba_2PrRuO_6$", *RSC Adv.*, **9** (2019) 12319–12324.
25. R. Das, R.N.P. Choudhary, "Structure, dielectric and electrical properties of relaxor lead-free double perovskite: $Nd_2NiMnO_6$", *Process. Appl. Ceram.*, **13** (2019) 1–11.
26. M. Afqir, M. Elaatmani, A. Zegzouti, N. Tahiri, M. Daoud, "Electrical properties of $SrBi_{2-y}Y_yNb_{2-x}V_xO_9$ (x/y = 0/0, 0/0.2, 0.05/0.1, 0.1/0.05 and 0.2/0) ceramics", *Appl. Phys. A*, **129** (2023) 191.
27. N. Bajpai, M. Saleem, S. Tiwari, M. Soni, A. Mishra, "Bismuth doped $La_2CoMnO_6$: A study of Williamson-Hall analysis and four-probe resistivity measurement", *AIP Conf. Proc.*, **2220** (2020) 040029.
28. R. Das, R.N.P. Choudhary, "Electrical and magnetic properties of double perovskite: $Y_2CoMnO_6$", *Ceram. Int.*, **47** (2021) 439–448.
29. R. Roy, A. Dutta, "Effect of vanadium doping on the electrical charge transport and dielectric relaxation properties of sodium bismuth titanate perovskite", *Ceram. Int.*, **47** (2021) 15732–15742.
30. R. Ranjan, R. Kumar, N. Kumar, B. Behera, R.N.P. Choudhary, "Impedance and electric modulus analysis of Sm-modified $Pb(Zr_{0.55}Ti_{0.45})_{1-x/4}O_3$ ceramics", *J. Alloys Compd.*, **509** (2011) 6388–6394.
31. F. Tian, Y. Ohki, "Electric modulus powerful tool for analyzing dielectric behaviour", *IEEE Transac. Dielectr. Elect. Insulat.*, **21** (2014) 929–931.
32. S. Karmakar, D. Behera, "Band-correlated barrier-hopping conduction in $\alpha$-$NiMoO_4$ micro-crystals and comparison of its energy storage performance with MWCNT-integrated complex", *J. Mater. Sci. Mater. Electron.*, **31** (2020) 5336–5352.